Biomaterials 159 (2018) 229–240

Contents lists available at ScienceDirect

Biomaterials

journal homepage: www.elsevier.com/locate/biomaterials

Generation of matched patient-derived xenograft *in vitro-in vivo* models using 3D macroporous hydrogels for the study of liver cancer

Eliza Li Shan Fong [a, *, 1], Tan Boon Toh [b, 1], Quy Xiao Xuan Lin [b, 2], Zheng Liu [c, 2], Lissa Hooi [b], Masturah Bte Mohd Abdul Rashid [b], Touati Benoukraf [b], Edward Kai-Hua Chow [b, j, **], The Hung Huynh [d, ***], Hanry Yu [c, e, f, g, h, i]

[a] *Department of Biomedical Engineering, National University of Singapore, Singapore*
[b] *Cancer Science Institute of Singapore, National University of Singapore, Singapore*
[c] *Institute of Bioengineering and Nanotechnology, Agency for Science, Technology and Research (A*STAR), Singapore*
[d] *National Cancer Center Singapore, Singapore*
[e] *Department of Physiology, Yong Loo Lin School of Medicine, National University of Singapore, Singapore*
[f] *Mechanobiology Institute, National University of Singapore, Singapore*
[g] *BioSyM, Singapore-MIT Alliance for Research and Technology, Singapore*
[h] *Department of Gastroenterology, Nanfang Hospital, Southern Medical University, Guangzhou, China*
[i] *NUS Graduate School of Integrative Sciences and Engineering, National University of Singapore, Singapore*
[j] *Department of Pharmacology, Yong Loo Lin School of Medicine, National University of Singapore, Singapore*

ARTICLE INFO

Article history:
Available online 4 January 2018

Keywords:
Hepatocellular carcinoma
Patient-derived xenograft
Drug testing
3D tumor model
Organoids

ABSTRACT

Hepatocellular carcinoma (HCC) is the third leading cause of cancer death worldwide, often manifesting at the advanced stage when cure is no longer possible. The discrepancy between preclinical findings and clinical outcome in HCC is well-recognized. So far, sorafenib is the only targeted therapy approved as first-line therapy for patients with advanced HCC. There is an urgent need for improved preclinical models for the development of HCC-targeted therapies. Patient-derived xenograft (PDX) tumor models have been shown to closely recapitulate human tumor biology and predict patient drug response. However, the use of PDX models is currently limited by high costs and low throughput. In this study, we engineered *in vitro* conditions conducive for the culture of HCC-PDX organoids derived from a panel of 14 different HCC-PDX lines through the use of a three-dimensional macroporous cellulosic sponge system. To validate the *in vitro* HCC-PDX models, both *in vivo* and *in vitro* HCC-PDX models were subjected to whole exome sequencing and RNA-sequencing. Correlative studies indicate strong concordance in genomic and transcriptomic profiles as well as intra-tumoral heterogeneity between each matched *in vitro-in vivo* HCC-PDX pairs. Furthermore, we demonstrate the feasibility of using these *in vitro* HCC-PDX models for drug testing, paving the way for more efficient preclinical studies in HCC drug development.

1. Introduction

Liver cancer is one of the leading causes of cancer death worldwide, with hepatocellular carcinoma (HCC) accounting for up to 90% of the disease [1]. While a third of HCC patients can benefit from resection, transplantation or local ablation, the remaining majority are diagnosed at advanced disease stages and are ineligible for such potentially curative treatments [2]. Given that advanced HCC is refractory to conventional chemotherapies, molecularly targeted therapies have been the mainstay treatment approach. However, at present, there are only two approved targeted therapies – multi-kinase inhibitors, sorafenib and regorafenib. Since the approval of sorafenib in 2007, several phase III trials conducted in the past decade investigating first-line and second-line agents have all failed to demonstrate superiority or

* Corresponding author.
** Corresponding author.
*** Corresponding author.
E-mail addresses: bieflse@nus.edu.sg (E.L.S. Fong), csikce@nus.edu.sg (E.K.-H. Chow), cmrhth@nccs.com.sg (T.H. Huynh).
[1] Co-First Authors.
[2] Co-Second Authors.

https://doi.org/10.1016/j.biomaterials.2017.12.026
0142-9612/

non-inferiority against sorafenib [3]; only recently (in 2017) was regorafenib approved for second-line use in HCC. This underscores the poor translation of encouraging results in preclinical studies to clinical outcomes in patients in the current drug development paradigm for HCC. It has been postulated that this discrepancy between preclinical and clinical drug response is due to the use of inadequate tumor models in preclinical studies [4,5].

Preclinical tumor models, largely comprising immortalized cancer cell lines that have adapted to *in vitro* culture over multiple passages on plastic, have been reported to undergo irreversible changes in gene expression and poorly represent the original tumor [5,6]. In addition to the accumulation of phenotypic changes that occur from repeated sub-culturing, cancer cell lines also undergo clonal selection. This results in the generation of highly homogeneous cancer cell populations that greatly misrepresent the intra-tumoral heterogeneity in patient tumors [7], a key clinical feature thought to determine treatment response and resistance in patients [8]. Particularly for HCC, as hepatocarcinogenesis arises from an accumulation of genetic and epigenetic aberrations of multiple cancer drivers over time in the context of different etiologies, each tumor harbors many low frequency-mutated genes in various combinations, making HCC a disease with high intra- and inter-tumoral heterogeneity in which several signaling cascades are altered [9,10]. This brings into question the clinical relevance of these heavily-used cell line-based HCC preclinical models [5] as they may not adequately recapitulate the heterogeneity in HCC tumors.

To address the need for improved tumor models, there has been a recent paradigm shift away from the use of cancer cell lines to patient-derived xenograft (PDX) *in vivo* models [4]. PDX models are powerful preclinical tumor models that preserve histopathological characteristics, genomic and transcriptomic profiles, tumor heterogeneity and drug response of patient tumors [4,11]. While highly relevant and thought to hold the potential to revolutionize anti-cancer drug development, PDX animal models are inherently time-consuming and costly, making them less than efficient models for preclinical studies. One possible solution is to grow PDX-derived cells *in vitro* to increase the throughput and reduce the use of animals. However, primary HCC cells are notoriously challenging to culture *in vitro*. Recently, a few groups reported the feasibility of culturing HCC-PDX cells *in vitro* [12,13]. However, these approaches involve growing the cells as adherent monolayers on flat tissue culture plastic which does not reflect the three-dimensional (3D) architecture of tumors and poorly supports the recapitulation of tumor microenvironment components (stromal cells and 3D extracellular matrix), diminishing the original translational value of these PDX models.

In this study, we embraced the challenge of generating matched *in vitro-in vivo* HCC-PDX models with concordant molecular features through a cross-disciplinary collaboration. We previously reported the capability to generate HCC-PDX models from HCC patients [14]. Since then, we have established 85 different HCC-PDX models of which a select group of 14 lines was used in this study. Importantly, all established models can be cryopreserved for subsequent re-engraftment and propagation, constituting a living HCC biobank that can be readily employed for drug screening. Using a bioengineering approach, we established robust *in vitro* conditions for the culture of cells derived from these HCC-PDX models as tumor organoids (henceforth referred to as HCC-3DPDX) using a 3D macroporous sponge fabricated from hydroxypropylcellulose (HPC). The 3D sponge system developed for this study is a modification of a previously published system designed for the culture of normal hepatocytes [15,16]; this is a cellulose-based hydrogel with interconnected macropores fabricated by leveraging the ability of HPC derivatives to undergo thermal-induced phase separation (TIPS) and photo-crosslinking. We previously demonstrated that the sponge macropores enable spheroid size control through physical constraint while conjugated galactose ligands and *in vivo*-like mechanical stiffness provide cues to normal hepatocytes to form spheroids with preserved hepatic morphology and functions [15]. However, fabrication of this sponge system is challenging as it involves the use of moisture-sensitive reagents (anhydrous chloroform) necessary for grafting allyl groups onto HPC to render the polymer photo-crosslinkable, generating batch-to-batch variations. In this study, we addressed this problem by replacing allyl as the photo-crosslinkable group with methacrylate (MA), as well as replacing the use of chloroform with dichloromethane as the solvent for the reaction to synthesize MA-HPC. Hypothesizing that this modified sponge system would be able to support the culture of cancerous hepatocytes, we report that majority of the HCC-PDX cells cultured within this bioengineered sponge remain viable, proliferative, and preserve the genomic and transcriptomic profiles as well as intra-tumoral heterogeneity of their *in vivo* counterparts.

2. Materials and methods

2.1. Synthesis of MA-HPC

In this study, instead of using allyl groups as the crosslinker for sponge fabrication [15,16], we used MA groups. HPC (M_n = 10 000 g/mol) and methacrylic anhydride (94%) were purchased from Sigma-Aldrich (Singapore), triethylamine (99%) was purchased from Merck (Singapore), dichloromethane (99.6% AR grade) and anhydrous diethyl ether (99%) were purchased from Fisher (Singapore). HPC (4 g, 11.75 mmol repeating units) was dissolved in dichloromethane (100 mL) and stirred rigorously. Following dissolution, methacrylic anhydride (3.48 mL, 2 equiv.) was added dropwise into the reaction mixture, followed by triethylamine (1.14 mL, 1 equiv.). The reaction mixture was stirred for 24 h, then quenched with 400 mL anhydrous diethyl ether. After washing twice with anhydrous diethyl ether, resulting fibers were filtered, collected and dried under rotovap for 30 min. The dried fibers were then re-dissolved in 200 mL deionized water and poured into dialysis tubes (MWCO = 14 kDa) for dialysis against running water for 48 h before lyophilization for 1 day. NMR characterization of MA-HPC is shown in Fig. 1A in Ref. [17].

2.2. Fabrication of sponge

MA-HPC was minced into small pieces and dissolved with water (10% w/v). The MA-HPC solution was then transferred into glass test tubes (6 mm diameter) and placed in a 1 L beaker filled with warm water (T = 42 °C). After 5 min, the beaker was placed in a rotating gamma radiator for 2.5 h (total dose = 5 kGy; Gammacell 220, MDS Nordion, Canada). Following irradiation, cross-linked MA-HPC hydrogel cylinders were obtained by breaking the test tubes. The hydrogel cylinders were sliced into thin pieces (1 mm) then lyophilized for 1 day. The MA-HPC sponge was then rinsed in dry acetone for 1 day, placed in vials filled with carbonyldiimidazole solution (0.13 g in 40 mL dry acetone) and then placed on a shaker overnight at 4 °C. The MA-HPC sponge slices were then washed in dry acetone (20 min each run, 3 times). Acetone in the vials was then removed and replaced with D-(t)-galactosamine HCl solution (0.08 g in 40 mL sodium bicarbonate buffer, pH = 10), and placed overnight on a shaker at 4 °C. The MA-HPC sponge slices were then washed in DPBS buffer (20 min each run, 3 times), followed by deionized water (20 min each run, 3 times) and then lyophilized.

2.3. Physicochemical characterization

2.3.1. Morphology

Top and cross section views of the sponge surface morphology were captured using SEM (JEOL JSM-5600, Japan) at 5 kV. Prior to imaging, the dried sponge was sputter-coated with platinum for 60 s.

2.3.2. UV transmission

The temperature-mediated phase behavior of MA-HPC in deionized water (10% w/v) was investigated using a UV/VIS/NIR spectrophotometer (Jasco, V-570, Japan) by measuring the optical densities at 480 nm as a function of temperature. The temperatures were controlled (heating rate of 0.1 K/min) using a Jasco PSC-498 temperature controller.

2.3.3. Porosity

Porosity of MA-HPC sponge was measured using Micromeritics AutoPore IV 9500 mercury intrusion porosimeter; value obtained was 94.8%. The porous morphology of hydrated sponge was visualized using propidium iodide staining. Sponge was incubated in 100 mg/mL propodium iodide in phosphate-buffered saline (PBS) overnight. Stained sponge was washed with PBS for 5 times before imaging was performed using the Olympus Fluoview FV1000 confocal microscope.

2.3.4. Young's modulus

The mechanical properties of hydrated sponge were evaluated by compression tests using an Instron Micro-Tester 5848 (Instron Co., U.S.A.), at a speed of 0.5 mm/min and 298 K. The Young's modulus was calculated from the slopes of the initial linear portion of stress-strain curves.

2.4. Generation and maintenance of HCC-PDX models

This study received ethics board approval at the National Cancer Center Singapore and SingHealth. All mice were maintained according to the Guide for the Care and Use of Laboratory Animals published by the National Institutes of Health, USA. We previously reported the capability to reliably generate primary HCC-PDX models using SCID mice for drug testing applications in HCC [14]. Since then, these HCC-PDX models have grown in numbers to comprise a living PDX biobank at the National Cancer Center Singapore, representative of HCC patients in the region and have been employed to evaluate the efficacy of various chemotherapeutic and targeted therapies against HCC [18–21]. Primary HCCs have previously been used to create PDX lines [14], of which 14 lines [25-0705A, 01-0207, 26-0808B, 01-0909, 13-0109, 29-0909A, 17-0211, 13-0212, 21-0114, 24-0714, 25-0914, 29-0714B, 26-0808A and 09-0913] were used to establish tumors in male SCID mice (In Vivo, Singapore) aged 9–10 weeks. For ease of reference, these 14 lines will be referred to as HCC 1-14.

2.5. Isolation and culture of HCC-PDX cells

HCC-PDX cells were harvested from the animals as previously published [20]. Tumors were finely minced and washed three times with modified Eagle medium (MEM). The minced tissue was incubated with MEM medium containing 5% fetal bovine serum (FBS) and 5 mg/mL collagenase (Roche Diagnostics Corporations, Indianapolis, IN, USA) at 37 °C for 12 h. Cells were harvested by centrifugation at 800g for 10 min and then passed through a 70 μm strainer. Cells were centrifuged again for 3 min and then counted. Each 3D sponge placed in a 24-well plate was seeded with 3×10^5 cells in 20 μL of medium, comprising DMEM supplemented with 10% FBS and 100 U/mL penicillin-streptomycin. 45min after seeding, 500 μL of medium was added to submerge the samples. Medium was replaced the next day with 1 mL of medium and every 2-3 days after.

2.6. Cell viability and growth assessment of HCC-3DPDX cultures

HCC-3DPDX samples were assessed for viability using calcein-AM (2 μM) and propidium iodide (25 μg/mL). Following a 30 min incubation with calcein-AM and propidium iodide, samples were immediately imaged using an Olympus Fluoview FV1000 or Zeiss LSM 710 confocal microscope. Samples were assessed for growth using CellTiter-Glo® (Promega) as described by the manufacturer.

2.7. Immunofluorescence staining of HCC-3DPDX

HCC-3DPDX samples were fixed with 4% paraformaldehyde for 30 min and stored in PBS at 4 °C. Samples were permeabilized with 0.3% Triton X-100 for 30 min, and blocked with 2% bovine serum albumin (BSA) in 0.1% Triton X-100 for 30 min. Following which, samples were incubated with primary anti-Ki-67 antibody (1:200, Merck) in 2% BSA overnight and subsequently washed with 0.1% Triton X-100 thrice with 15 min for each wash. Samples were then incubated with goat anti-rabbit secondary antibody (1:200, Abcam), phalloidin and DAPI in 2% BSA for 2 h and subsequently washed again thrice with 15 min for each wash. Samples were then mechanically torn to release the tumor organoids for imaging. All imaging was performed using the Olympus Fluoview FV1000 or Zeiss LSM 710 confocal microscope.

2.8. Whole exome sequencing and RNA-sequencing data analysis

HCC-PDX and HCC-3DPDX samples were both sequenced by Auragen Pte Ltd, Singapore. For whole exome sequencing (WES) (using HiSeq 4000-150PE), short reads were aligned to hg19 with BWA [22] and duplicated reads were removed with Picard (Broad Institute). Improvement of alignments and genetic variants calling were completed using Genome Analysis Toolkit (GATK) [23]. Overlaps of SNP and INDEL between HCC-PDX and HCC-3DPDX were analyzed using VCFtools [24]. To investigate whether HCC-3DPDX retains key mutations in HCC, we referred to 32 known HCC driver genes [10] for genetic variant annotation achieved by ANNOVAR [25]; mutation types are divided in two groups, synonymous mutation and nonsynonymous/indel mutation, latter of which includes frameshift deletion, frameshift insertion, nonframeshift deletion, nonframeshift insertion, nonsynonymous SNV, stopgain and stoploss. To investigate whether intra-heterogeneity is retained in HCC-3DPDX, we used variant allele frequency as a surrogate measure. For each genetic variant locus, variant allele frequency is the ratio of altered allele number to detected total number.

For RNA-sequencing (RNA-seq) data (using HiSeq 2500-100PE), raw reads were aligned to the human reference genome using STAR [26]. Fragment per kilobase of transcript per million mapped reads (FPKM), a gene expression measure, was calculated for each gene by HOMER [27]. To investigate whether HCC-PDX and HCC-3DPDX share similar gene expression profiles, we focused on 219 up-regulated and 514 down-regulated genes known to be dysregulated in HCC [28]. Comparative analysis was performed using Pearson correlation (gene expression measure FPKM underwent *asinh* transformation). To verify this, using the same strategy, we also compared the similarity in gene expression of known HCC dysregulated pathways between HCC-PDX and HCC-3DPDX. Based on KEGG [29], nine cancer related pathways, namely AKT, Hedgehog, Hippo, Notch, p53, Ras, TGF-beta, VEGF and Wnt pathways, as

well as the overall pathways in cancer, were analyzed.

2.9. Drug treatment

HCC-3DPDX samples were cultured for 5 days before treatment with Sorafenib (Nexavar) or BGJ-398 for 48 h. Following which, samples were collected for CellTiter-Glo® assay. To determine changes in indicated proteins, HCC-3DPDX samples were collected following 48 h of drug treatment. Lysates of 4–5 samples from each group were pooled. Each lane represents one protein pool (30 mg of proteins). Antibodies used for immunoblot analyses included for p-Akt (Ser 473) (1: 1000, Cell Signaling), total Akt (1:1000, Cell Signaling), p-Erk1/2 (1:1000, Cell Signaling), total Erk1/2 (1:1000, Cell Signaling) and β-actin (1:5000, Sigma). The blots were then visualized with a chemiluminescent detection system as described by the manufacturer.

3. Results

3.1. Synthesis and characterization of cellulosic sponge

The ability of HPC to undergo TIPS from an isotropic aqueous to meta-stable bi-phasic state enables the unique fabrication of 3D macroporous sponge-like hydrogels by crosslinking its derivatives during phase separation [16]. To render HPC photo-crosslinkable, we reacted the polymer with MA and verified the grafting of MA groups (degree of substitution, 5.8%) using NMR (see Fig. 1A in Ref. [17]). The resulting MA-HPC derivative retains the ability to undergo TIPS without any noticeable sedimentation (Fig. 1A). The colloidal structure that forms during TIPS is then 'fixed' through the use of gamma-irradiation, giving rise to a macroporous sponge (Fig. 1B).

As shown in the scanning electron micrograph in Fig. 1C, the sponge has a highly macroporous structure (pore size: 80-180 μm, see Fig. 1B in Ref. [17] for pore size distribution; porosity 94.8%) which is consistent throughout the sponge cross-section, enabling the formation of cellular organoids within diffusion limits [30]. This macroporosity is maintained whether the sponge is dry or hydrated (Figs. 1C and D). Besides having mechanical properties (modulus of 9.7 kPa) similar to *in vivo* liver [31], the sponge is also conjugated with galactose moieties (see Fig. 1C in Ref. [17]) to promote organoid formation and tethering to the sponge surface. Receptor-mediated interaction between asialoglycoprotein receptor on hepatocytes and galactose moieties is known to guide hepatocyte adhesion [32]. To test whether the sponge supports the organoid formation of HCC-PDX cells, we harvested HCC-PDX tumors grown in the animal, dissociated the tumor, and seeded single HCC-PDX cells onto the sponge. As hypothesized, these cells aggregated to form organoids within the physical constraints of the sponge macropores, suggesting that the sponge may be conducive for the culture of HCC-PDX cells *in vitro* (Fig. 1E).

3.2. HCC-3DPDX cells remain viable and proliferative in vitro

Given that the 3D sponge supports the formation of HCC-PDX organoids, we next asked if this finding is universal to most HCC-

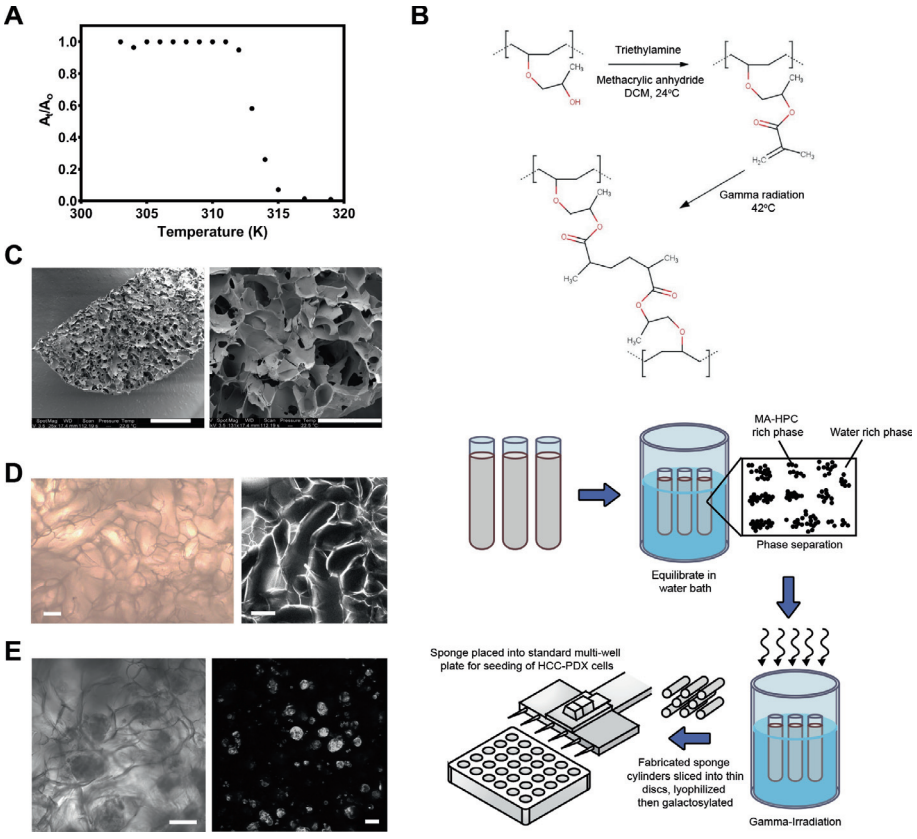

Fig. 1. Characterization of MA-HPC polymer and sponge fabrication. (A) Normalized UV absorption as MA-HPC undergoes thermal-induced phase separation with increasing temperature. Aqueous MA-HPC exhibits low critical solution temperature transition, from isotropic solutions at room temperature to metastable colloidal systems upon heating. Phase transition occurs at the precipitous decrease in transmittance with increasing temperature. **(B)** Reaction scheme of MA-HPC and sponge fabrication process. **(C)** Scanning electron micrographs of MA-HPC sponge at low (left, scale bar = 1 mm) and high (right, scale bar = 300 μm) magnifications, highlighting macroporosity of sponge. **(D)** Brightfield image of MA-HPC image when dry (left) and hydrated (right, stained with propidium iodide). **(E)** Brightfield (left) and phalloidin-stained (right) images of HCC-PDX cells cultured in MA-HPC sponge. Scale bars = 100 μm.

PDX lines and whether cells remain viable and proliferative in culture, the latter being critical for assessing drug candidates that target proliferating cancer cells. To this end, we assessed the viability of 16 different HCC-PDX lines using a viability stain comprising calcein-AM and propidium iodide, which stains viable cells green and dead cells red, respectively. Fig. 2A shows the viability of six representative HCC-PDX lines; cells rapidly formed organoids by Day 2 (see Fig. 2A in Ref. [17]) and remained largely viable through one week in culture; the same was found for approximately 75% of the HCC-PDX lines (see Fig. 3A in Ref. [17], data not shown for 2 of the 16 lines which did not survive) evaluated. For a few lines, viability could be maintained for almost three weeks in culture (see Fig. 2B in Ref. [17]). We verified this quantitatively with CellTiter-Glo® (Fig. 2C and Fig. 4 in Ref. [17]) by using ATP content as a surrogate measure of cell number and found that cell numbers were largely maintained for the HCC-PDX lines that appeared viable by staining. Moreover, by probing for Ki-67 expression, we found that even though there was a lack of significant measurable growth during two weeks of culture, all HCC-PDX lines formed organoids with varying proportions of Ki-67$^+$ cells, indicating that the *in vitro* conditions maintain the proliferative potential of the cultured HCC-PDX cells (Fig. 2B and Fig. 3B in Ref. [17]).

In summary, the inability to support all HCC-PDX lines in culture reflects the expected inter-tumoral diversity that exists among HCC patients and the immense difficulty of developing conditions that are conducive for the culture of heterogeneous primary HCC cells, as is well-recognized in the field. In subsequent studies, we only characterized 14 matched *in vitro-in vivo* HCC-PDX lines that remained viable in our culture system. Matched pairs were comprehensively characterized using WES and RNA-seq to determine the degree of genomic and transcriptomic correlation, as well as retention of intra-tumoral heterogeneity.

3.3. HCC-3DPDX retain global genomic profile and mutational signature of in vivo counterpart

The extent to which these matched *in vitro-in vivo* HCC-PDX

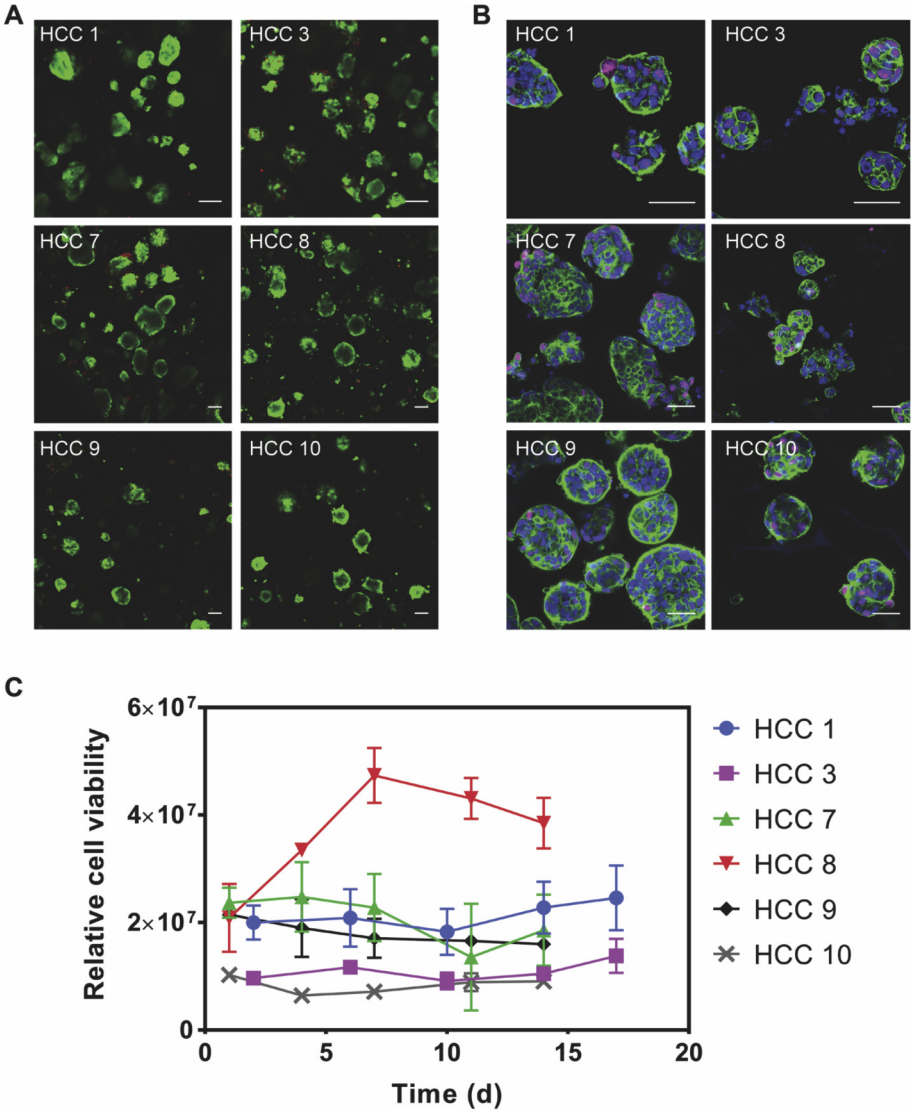

Fig. 2. Viability and growth profile of representative HCC-3DPDX models. (A) Viability staining of cells derived from six different HCC-PDX lines cultured in MA-HPC sponge for 7 days. Viable cells were labeled green by Calcein-AM and dead cells were labeled red by propidium iodide. Scale bars = 100 μm. **(B)** Ki-67 expression in proliferating cells, indicated in magenta. Cells were also stained with DAPI (blue) and phalloidin (green) to indicate location of nucleus and actin (to visualize morphology of organoids), respectively. Scale bars = 50 μm. **(C)** Relative viability of cells derived from the six different HCC-PDX lines cultured in MA-HPC sponge over two weeks in culture, as indicated by ATP content using CellTiter-Glo®.

lines is useful for the study of HCC is dependent on the fidelity of the HCC-3DPDX models in recapitulating the molecular phenotype (key genomic aberrations and signaling pathways) of their *in vivo* counterparts. We first determined the degree of genomic concordance by subjecting matched *in vitro* and *in vivo* models to WES, followed by SNP and INDEL calling. SNPs are genetic variations that occur naturally in the human genome. An insertion/deletion polymorphism, or INDEL, is a type of genetic variation in which a specific nucleotide sequence is present or absent. The extent of SNP and INDEL overlap was used to determine the degree of genomic concordance between matched pairs. As shown in Fig. 3A and B (also see Table 1 in Ref. [17]), high SNP and INDEL concordance was observed between matched *in vitro-in vivo* pairs for all HCC-PDX lines, except one line (HCC4-PDX). Furthermore, mutational signatures [33] were also conserved (see Fig. 6 in Ref. [17]). This indicates that culture of HCC-PDX cells within the sponge enables the retention of global genomic features of their *in vivo* counterpart.

Several groups have probed into the genomic landscape of HCC to identify genes that are recurrently altered in HCC and play critical role in pathways involved in hepatocarcinogenesis, including tumor suppressor genes *TP53*, *RB1* and *AXIN1* that are inactivated, the Wnt pathway oncogene *CTNNB1* and chromatin remodeling genes *ARID1A* and *ARID2*, amongst several others [10]. Focusing specifically on these key HCC mutations, we demonstrated that HCC-3DPDX cells largely recapitulated these genomic alterations found in their corresponding *in vivo* counterpart (Fig. 3C). In summary,

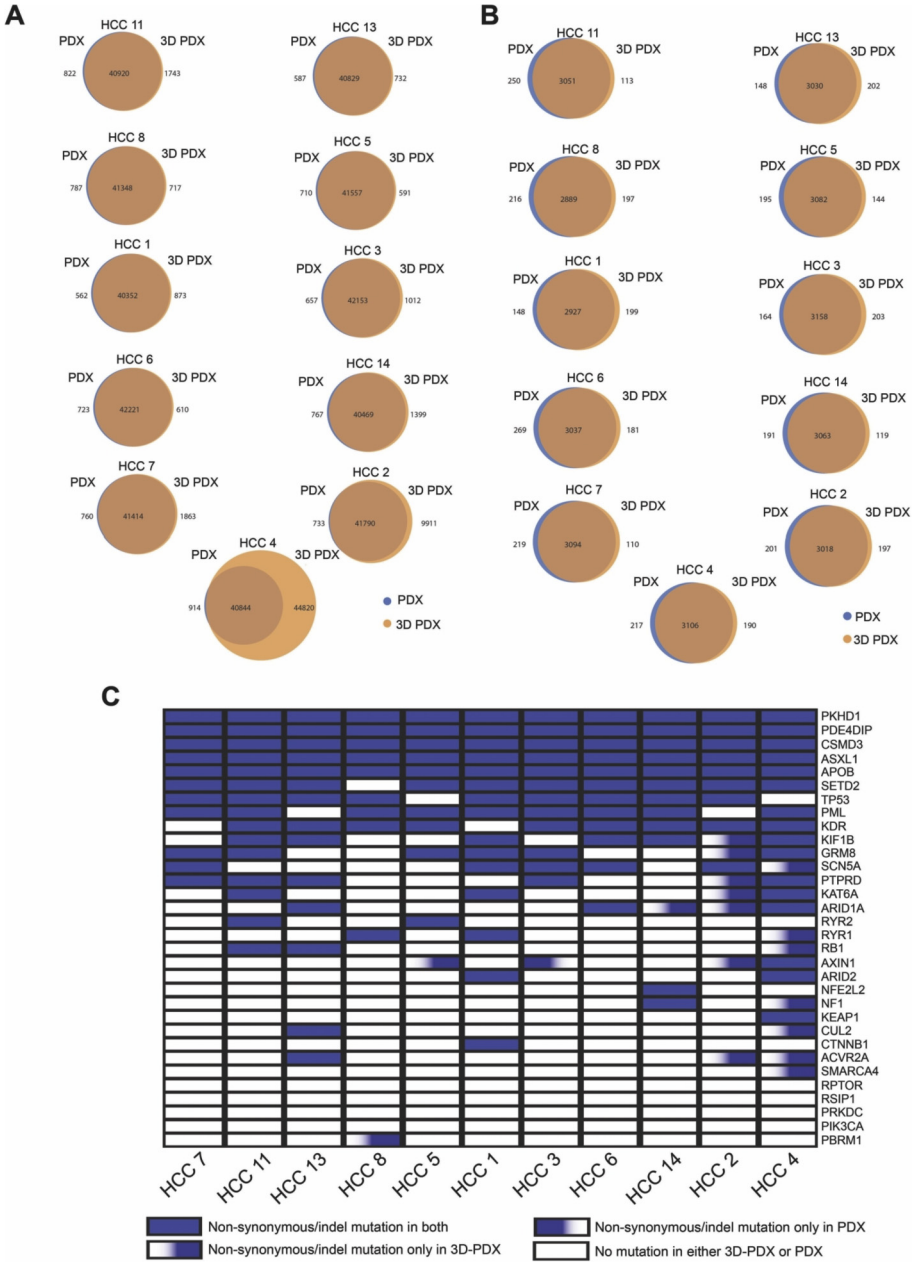

Fig. 3. Genomic correlation between matched *in vitro-in vivo* HCC-PDX models (A) SNP and **(B)** INDEL overlap between PDX (*in vivo*) and 3D PDX (*in vitro*) for 11 HCC-PDX lines. **(C)** Mutational profile of PDX and 3D PDX. List of known HCC driver genes with non-synonymous/indel mutations are shown on the right. Each column in the grid represents the mutational profile of a matched *in vitro-in vivo* HCC-PDX line, and each row represents a driver gene. White box indicates no mutation present; fully-shaded blue box indicates mutation is present in both PDX and 3D PDX; blue-shading on right of box indicates mutation present only in 3D PDX; blue-shading on left of box indicates mutation present only in PDX. Except for HCC 2 and 4, majority of matched *in vitro-in vivo* pairs share similar mutational profiles.

our findings robustly demonstrate preservation of genomic profile when HCC-PDX cells are cultured in our 3D sponge.

3.4. HCC-3DPDX retain gene expression profile of their in vivo counterpart

Given the strong genomic concordance between HCC-PDX cells grown in our sponge system and *in vivo*, we next asked how *in vitro* culture affects gene expression, considering that several tumor microenvironmental cues, including vasculature and other stromal components, are absent in culture. Subjecting both sponge-cultured HCC-PDX cells and matched *in vivo* tissue to RNA-seq, we determined the degree of correlation between the matched pairs by focusing on a set of known HCC dysregulated genes. Ho and colleagues previously evaluated The Cancer Genome Atlas (TCGA) whole transcriptome sequencing data of HCC by comparing the global gene expression profiles of tumor and corresponding normal liver tissue; gene set enrichment analysis (GSEA) indicated that various genes associated with cell cycle processes were frequently up-regulated, while genes associated with metabolic processes such as metabolism of retinol, amino acids, and carbohydrates were preferentially down-regulated in HCC [28]. Focusing on these reported up- and down-regulated genes, we performed Pearson correlation analysis on matched *in vitro-in vivo* HCC-PDX pairs and found that the correlation coefficient was on the average 0.8 (Fig. 4A, and Figs. 8A and B in Ref. [17]), suggesting strong correlation in gene expression between the two models despite the lack of supporting stromal components.

Variations in the degree of *in vitro-in vivo* gene expression correlation (Fig. 4A) amongst the different HCC-PDX lines indicate that the *in vitro* conditions established in this study support the preservation of *in vivo* gene expression to different extents (PDX line-dependent). This suggests that different HCC-PDX lines may have unique requirements for growth, as would be expected given that

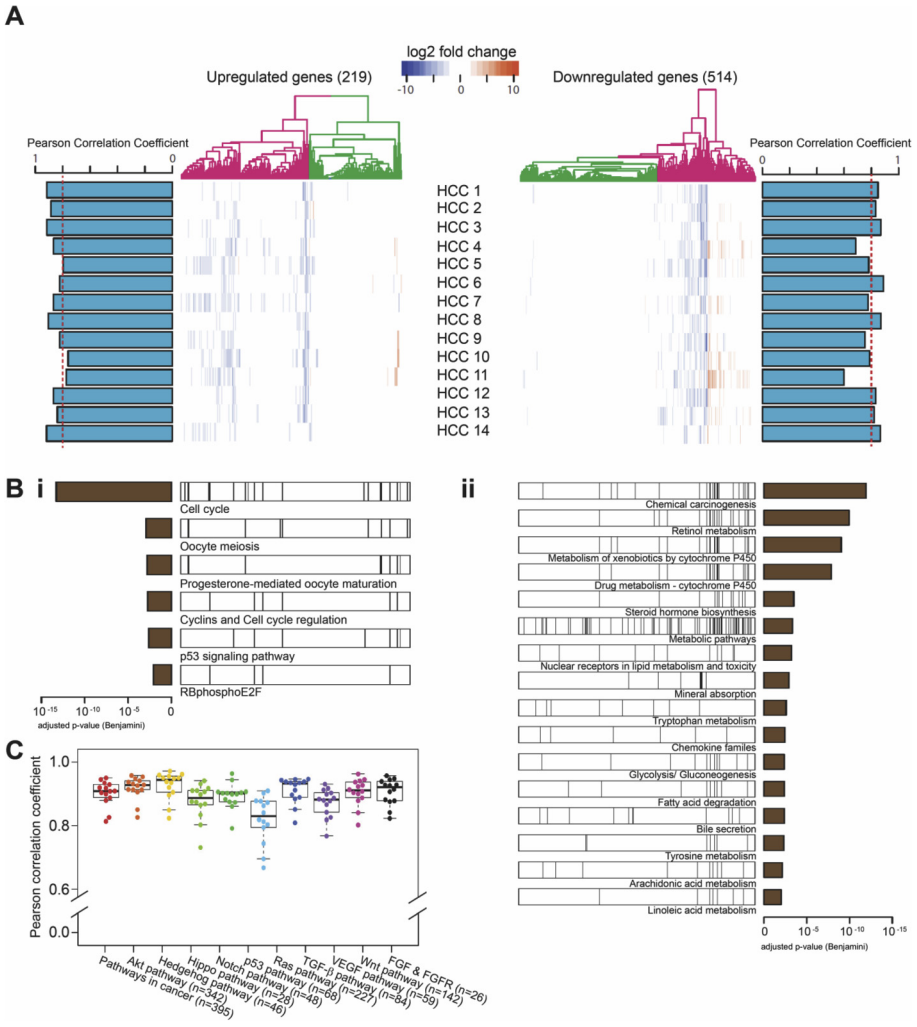

Fig. 4. Transcriptomic correlation between matched *in vitro-in vivo* HCC-PDX models (A) Heatmaps of fold change differences (PDX vs 3D PDX) in expression levels (FPKM) of known up-regulated and down-regulated HCC genes between PDX and 3D PDX. Each row in the heatmap represents the expression profile of individual HCC-PDX lines (HCC 1-14). Each column represents a gene. Blue lines in the heatmap indicate lower gene expression in PDX as compared to 3D PDX and red lines indicate higher gene expression in PDX as compared to 3D PDX. Globally, the heatmaps for both down-regulated and up-regulated genes are largely white, indicating similarity in gene expression profile between PDX and 3D PDX. This was quantified using Pearson correlation coefficient as indicated by the blue bars on the left (refer to Fig. 8A in Ref. [17] for details) and right (refer to Fig. 8B in Ref. [17] for details) of the heatmaps. **(B) i.** Differentially expressed genes (up-regulated in HCC) between PDX and 3D PDX are significantly enriched in cell cycle and p53 signaling pathways amongst others (brown bars). **ii.** Differentially expressed genes (down-regulated in HCC) between PDX and 3D PDX are significantly enriched in metabolism-related pathways amongst others (brown bars). Black lines represent individual genes in these enriched pathways, where their position along the white bar corresponds to their position in the heatmap in **(A)**. **(C)** Beeswarm plot of Pearson correlation coefficient between PDX and 3D PDX for nine cancer-related pathways and overall pathways in cancer. Each dot represents a matched *in vitro-in vivo* HCC-PDX pair.

each of these PDX lines were derived from individual patients (an indication of inter-tumoral heterogeneity). Noting significant fold changes in gene expression comparing the two groups in certain genes (represented by red and blue lines in the heatmaps, Fig. 4A), we asked if these differences in gene expression between matched HCC-PDX *in vitro* and *in vivo* models might potentially influence important cancer-associated pathways. Pathway analysis was performed using hypergeometric test with adjusted p-value (Benjamini) threshold set as 0.01, to associate the differentially expressed genes reported by Ho et al. [28] with signaling pathways (Fig. 4B). We found that in the set of up-regulated genes, the p53 signaling pathway was significantly enriched with 7 genes involved (adjusted p-value < .01, Fig. 4Bi), but 6 out of these 7 genes preserved their expression patterns when HCC-PDX cells were grown in our sponge system (Fig. 4A and Bi). However, we also found that the majority of the enriched pathways in the set of down-regulated genes were metabolic processes-related, and most of the genes in these pathways were different in expression levels between matched HCC-PDX *in vivo* and *in vitro* models (Fig. 4A and Bii). This suggests that metabolic adaptation of the HCC-PDX cells might have occurred in our sponge system. Lastly, we verified the analysis done in Fig. 4A by focusing on genes in known oncogenic pathways. Comparing the expression of 395 genes in cancer-associated pathways *in vitro* and *in vivo*, Pearson correlation coefficient was high at approximately 0.9 (Fig. 4C). Furthermore, analysis of genes in specific HCC-associated pathways such as tumor protein p53 (TP53), Wnt, and Ras amongst others indicate a tight range in the degree of correlation (all greater than 0.8) between HCC-PDX grown *in vitro* and *in vivo* (Fig. 4C), confirming that HCC-PDX grown *in vitro* closely match the gene expression profile of the corresponding *in vivo* HCC-PDX. In summary, characterization of genomic aberrations and gene expression of the various HCC-PDX lines grown *in vitro* confirms these models have a striking molecular resemblance to their corresponding matched *in vivo* counterpart.

3.5. Intra-tumoral heterogeneity of HCC-PDX cells is retained in culture

HCC is a disease with high intra-tumoral heterogeneity in which several signaling cascades are altered [9]. We used WES data to determine whether HCC-PDX cells grown in our sponge system retain the intra-tumoral heterogeneity inherent in their matched *in vivo* counterpart. Quantification of variant allele frequency as a surrogate measure of intra-tumoral heterogeneity revealed that the *in vivo* HCC-PDX models had a range of scores, as expected given their diversity (indicated by the genomic and transcriptomic analyses above). A score of 100% indicates that there is no heterogeneity present while a score of less than 100% indicates the presence of sub-clonal populations. As shown in Fig. 5, the variant allele frequency scores in matched *in vitro* and *in vivo* models were similar for 9 out of 11 HCC-PDX lines, highlighting that *in vitro* HCC-PDX models largely capture the intra-tumoral heterogeneity of their *in vivo* counterparts. Notably, the mismatch in variant allele frequency for HCC4-PDX corroborates with the poor SNP and INDEL overlap (Fig. 3) as well as gene expression correlation (Fig. 4A) observed, suggesting that for this particular line, the sponge system is not able to maintain the clonal dynamics of the *in vivo* tumor. Nevertheless, contrary to what is expected of *in vitro* culture (that there would be clonal selection resulting from adaptation to *in vitro* culture conditions), overall, our data suggests that the sponge system well-preserves the intra-tumoral heterogeneity of the corresponding *in vivo* counterpart for the majority of HCC-PDX lines.

3.6. HCC-PDX cultures are amenable for drug testing in vitro

To evaluate the feasibility of using these HCC-PDX cells grown in our 3D macroporous sponge for drug assay development, we

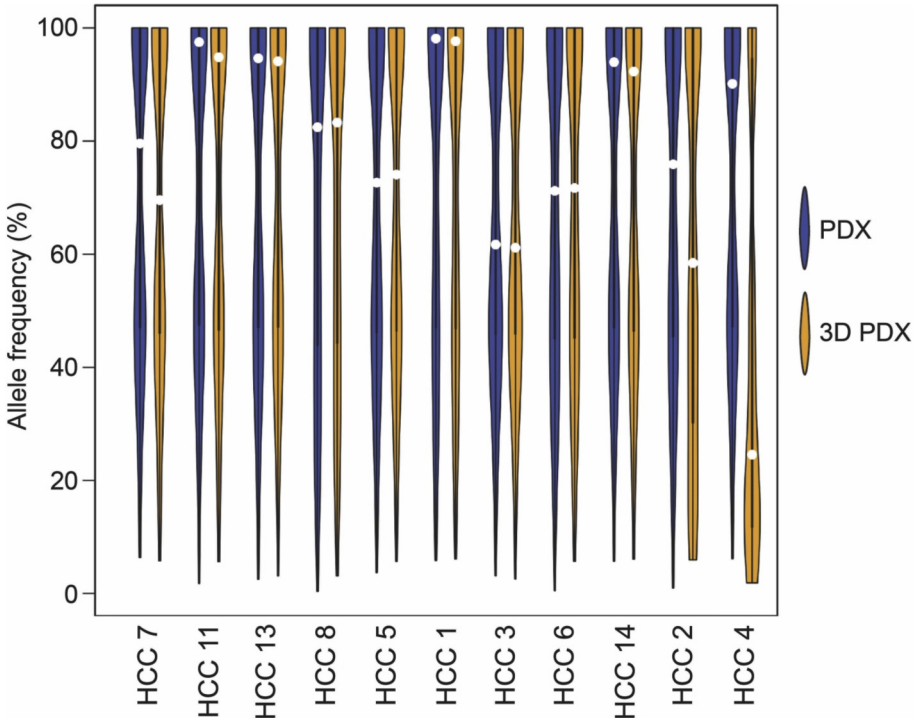

Fig. 5. Extent of intra-tumoral heterogeneity retention in HCC-3DPDX Violin plot of variant allele frequencies of all genetic variants in PDX and 3D PDX. White dots indicate the median variant allele frequency. Except for HCC 2 and 4, the majority of *in vitro-in vivo* HCC-PDX pairs share similar allele frequency profiles.

employed the use of Sorafenib (Nexavar) and BGJ-398. Sorafenib is an FDA-approved multi-kinase inhibitor for advanced HCC patients [34] whereas BGJ-398 is a pan-fibroblast growth factor receptor (FGFR) inhibitor which has been explored for use in certain subclasses of HCC [35]. *In vitro* drug treatment on HCC-3DPDX organoids showed dose-dependent decrease in cell viability, with cell kill of 87% and 37% at the highest concentration for Sorafenib and BGJ-398, respectively (Fig. 6A). In addition, an immunoblot analysis on these treated cells showed dose-dependent decrease in the levels of phosphorylated-Erk and a significant decrease in phosphorylated-Akt levels in response to Sorafenib and BGJ-398 respectively (Fig. 6B) as previously reported [20,36]. Our data suggests that HCC3-3DPDX is sensitive to both Sorafenib and BGJ-398, and that HCC-PDX cells grown in our sponge system can potentially be used for HCC drug discovery and development.

4. Discussion

The recent paradigm shift away from the use of cancer cell lines has catapulted PDX models as the gold standard for use in preclinical studies and drug development [4,37]. The use of PDX models is particularly important for cancers such as HCC, which has extensive heterogeneity of which individual cancer cell lines are largely unable to recapitulate. While PDX models are highly relevant, the use of these models for high throughput drug studies is significantly limited by the demanding nature of the model, requiring high costs and lengthy experimental durations. To overcome this problem, efforts have been made to develop *in vitro* counterparts to PDX models, which not only increase the throughput of experiments, but potentially also reduce costs and alleviate animal welfare concerns [38,39]. However, the same has yet been achieved for HCC as primary HCC cells are notoriously challenging to culture *in vitro*; there are only very few reports in the literature describing *in vitro* culture conditions for HCC cells derived either directly from patients [9,40], or from HCC-PDX models [12,13]. Specifically, Cheung et al. [12] and Xin et al. [13] reported the establishment of cell lines from HCC-PDX models. However, phenotypic characterization and correlation with the corresponding *in vivo* PDX models were limited in these studies, making it challenging to assess the fidelity of these 2D HCC-PDX models in recapitulating the HCC-PDX *in vivo* phenotype. Furthermore, these methods generally involve the use of adherent monolayer culture, which has been linked to clonal selection, acquisition of genetic alterations and changes in gene expression [5,6,40]. In the past few decades, numerous studies have shown that 2D cultures are not representative of the *in vivo* situation [41–43]. Particularly for HCC, studies have shown that drug response between 2D and 3D cell cultures are different, where cells in 3D cultures were found to be more resistant than those in 2D cultures [44]. Additionally, HCC cells grown in 3D were also found to be more tumorigenic than those grown in 2D [45]. Hence, in this study, we chose to focus only on developing 3D conditions amenable for the culture of HCC-PDX organoids. To our knowledge, we are one of the first to establish robust 3D *in vitro* culture conditions that supports the culture of HCC-PDX lines, with retained viability, proliferative capacity, genomic profile, gene expression and intra-tumoral heterogeneity.

In seeking to develop *in vitro* conditions suitable for the culture of HCC-PDX organoids, we asked whether existing 3D platforms that have been shown to be conducive for the culture of normal hepatocytes would similarly support the culture of cancerous HCC-PDX cells. Various methods are available to culture hepatocytes in 3D [46]. However, these approaches generally do not provide appropriate biochemical and mechanical cues necessary to maintain hepatocyte function. We previously reported the development of a macroporous cellulosic sponge system specifically engineered for the culture of normal hepatocytes as constrained spheroids with preserved hepatic morphology and functions based on *in vivo*-like mechanical and biochemical properties [15]. However, fabrication of this sponge system is challenging due to the use of moisture-sensitive reagents (anhydrous chloroform) which may generate batch-to-batch variations. Accordingly, in this study, we replaced allyl as the photo-crosslinkable group to MA, as well as replaced the use of chloroform with dichloromethane as the solvent for the reaction (Fig. 1B) to synthesize MA-HPC as the HPC derivative that undergoes TIPS and crosslinking. As shown in Fig. 1A, MA-HPC retains the ability to undergo TIPS, which we 'fixed' using photo-crosslinking via gamma irradiation. The resulting sponge system remains highly macroporous, with porosity, mechanical and biochemical properties similar to our previously developed sponge system [15]. Notably, individual sponge pieces are fabricated thin to minimize drug adsorption and to support high throughput applications, similar to conventional multi-well plates. Importantly, we found that this sponge system was able to support the rapid

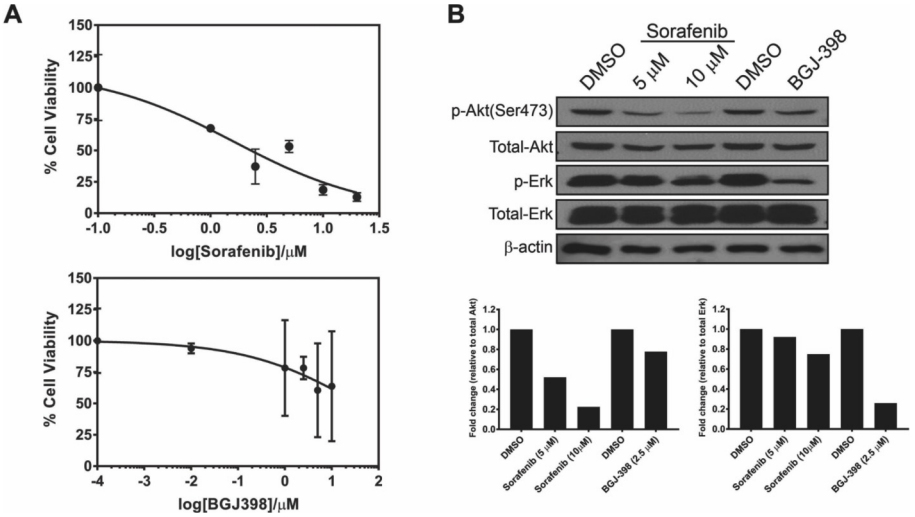

Fig. 6. Evaluation of standard and experimental drug response on HCC-3DPDX Response of HCC3-PDX to sorafenib and BGJ-398 as assessed by **(A)** CellTiter-Glo® and **(B)** western blot.

organoid formation of HCC-PDX cells and maintain the viability and proliferative capacity of the majority of HCC-PDX lines we tested (Fig. 2). Furthermore, each HCC-PDX *in vivo* model can give rise to tens to hundreds of HCC-3DPDX samples, greatly expanding the throughput of the PDX model. Extrapolation of *in vitro* conditions established for normal cells to cancer cells is an approach that has been explored for tumor engineering [41,47] and our data strongly supports this, suggesting that other cancers may also benefit from such an approach.

While we observed the presence of proliferative (Ki-67^{+}) cells, the lack of measurable cell growth during culture was perplexing. We suspect that there is a sub-population of cells that are dying as well during culture. Hence, there is cell turnover which maintains cell number over time. A similar observation was previously reported with prostate cancer PDX cells in 3D culture [39]. Additionally, the physical constraint exerted by the macropores of the sponge may have limited the proliferation of the HCC-PDX organoids. Incorporating degradability into the sponge system, such as through the use of matrix metalloproteinase-sensitive moieties, may potentially resolve this issue. Beyond being able to maintain the culture of HCC-PDX organoids, our data clearly demonstrates the strong concordance in genomic and gene expression profiles between matched *in vitro-in vivo* HCC-PDX pairs (Figs. 3 and 4). Using SNP and INDEL calling and mutational signatures, we found that 10 out of 11 of the *in vitro-in vivo* HCC-PDX pairs shared similar genomic profiles, except for HCC4-PDX. Not unexpected, HCC4-3DPDX also poorly recapitulated known HCC mutations such as *NF1*, *CUL2* and *ACVR2A*. This was confirmed by subsequent analysis indicating that HCC4-3DPDX poorly correlated with its *in vivo* counterpart in terms of expression levels of known dysregulated HCC genes (Fig. 4), as well as its inability to maintain *in vivo* levels of intra-heterogeneity (Fig. 5). Comparing gene expression profiles, that metabolism-related genes surfaced as significantly different between the *in vivo* and *in vitro* models (Fig. 4B) suggests that our existing 3D sponge system is yet able to support *in vivo*-like metabolic activities. Schutte and colleagues reported that patient-derived colorectal cancer organoids grown in culture exhibited differential expression of genes involved in carbohydrate, steroid, retinoid and fatty acid metabolism as compared to the PDX *in vivo* model and original patient tumor [48], implying that metabolic adaption to cell culture conditions may be an intrinsic consequence of *in vitro* culture.

It is possible that clonal selection might have occurred for HCC4-PDX when grown in our sponge system. Indeed, Qiu and colleagues showed that early-passage patient-derived HCC cells when grown in culture gain approximately half of total new mutations *in vitro*, attributing this to clonal selection of HCC cells during culture [40]. Notably, cancer cell adaptation resulting in changes in clonal architecture also occurs for organoid culture [49], and even PDX *in vivo* models [11], highlighting the challenge of developing *in vitro* conditions suitable for maintaining primary cancer cells. In contrast to conventional spheroid-generating methods such as the hanging drop technique or ultra-low attachment surfaces, our 3D bioengineered sponge enables control over biochemical and mechanical cues needed to recapitulate the tumor microenvironment. Ongoing investigations are being undertaken in our laboratory to modify the biochemical and mechanical properties of our sponge system to accommodate the culture of HCC-PDX lines such as HCC4-PDX with unique growth requirements. For example, the mechanical properties of the sponge may be modulated by changing the degree of MA grafting onto the HPC polymer backbone, or changing the duration of gamma irradiation or concentration of the MA-HPC solution used for sponge fabrication. Nevertheless, despite the complexity of the HCC microenvironment – an ecosystem comprising various players (stromal cells and the dynamic extracellular matrix) that shape the cancer cell phenotype spatiotemporally [50] – that the majority of the HCC-PDX lines evaluated in this study conserved key molecular features including intra-tumoral heterogeneity uniquely positions our sponge system as a novel platform for primary HCC culture with high translational value for the study of HCC and drug development.

In summary, we demonstrated the feasibility of using a 3D macroporous sponge system to maintain HCC-PDX organoids *in vitro*, which increases the cost-effectiveness and throughput of current HCC-PDX *in vivo* models for preclinical drug development in HCC.

Potential conflict of interest

Pishon Biomedical Co. Ltd and Invitrocue Ltd have licensed technology relevant to the class of cellulose sponge materials from ETPL, A*STAR and H.Y. has equity in these companies. There is no other conflict of interest otherwise.

Author contributions

E.L.S.F. conceived the experiments and wrote the manuscript. E.L.S.F., T.T.B and T.H.H. carried out the experiments. Z.L. designed and fabricated the sponge. All bioinformatics analyses in this study were designed by T.B. and performed by X.L. L.H. and M.R. provided technical support. E.L.S.F., T.T.B. E.K-H.C, T.H.H. and H.Y. contributed to the interpretation of the results and provided critical feedback and helped shape the research, analysis and manuscript.

Acknowledgements

T.H. Huynh would like to acknowledge funding from the National Medical Research Council of Singapore (NMRC/MOHIAF-CAT2/006/2016). E.K-H. Chow would like to acknowledge funding from the National Research Foundation Cancer Science Institute of Singapore RCE Main Grant, Ministry of Education Academic Research Fund (MOE AcRF Tier 2, MOE2015-T2-2-126, Seed Fund Grant T1-BSRG 2014–05) and NMRC Translational and Clinical Research (TCR) Flagship Programme (NMRC/TCR/015-NCC/2016). H. Yu would like to acknowledge funding from the Mechanobiology Institute (National University of Singapore, Singapore, Grant number: R-714-006-008-271), Institute of Bioengineering and Nanotechnology (A*STAR, Singapore), Singapore-MIT Alliance for Research and Technology, National Medical Research Council (Ministry of Health, Singapore, Grant Number: R-185-000-294-511) and Joint Council Office grants (A*STAR, Singapore). We would also like to acknowledge Dr. Melanie Lee (Mechanobiology Institute, National University of Singapore) for her help with graphic illustration, and the National University Health System Confocal Microscopy Unit for help with confocal microscopy.

References

[1] L.A. Torre, F. Bray, R.L. Siegel, J. Ferlay, J. Lortet-Tieulent, A. Jemal, Global cancer statistics, 2012, CA A Cancer J. Clin. 65 (2) (2015) 87–108.
[2] J.M. Llovet, A. Villanueva, A. Lachenmayer, R.S. Finn, Advances in targeted therapies for hepatocellular carcinoma in the genomic era, Nat. Rev. Clin. Oncol. 12 (7) (2015) 408–424.
[3] N. Goossens, X. Sun, Y. Hoshida, Molecular classification of hepatocellular carcinoma: potential therapeutic implications, Hepatol. Oncol. 2 (4) (2015) 371–379.
[4] H. Ledford, US cancer institute to overhaul tumour cell lines, Nature 530 (7591) (2016) 391.
[5] W. Wang, N.G. Iyer, H.T. Tay, Y. Wu, T.K. Lim, L. Zheng, I.C. Song, C.K. Kwoh, H. Huynh, P.O. Tan, P.K. Chow, Microarray profiling shows distinct differences between primary tumors and commonly used preclinical models in hepatocellular carcinoma, BMC Canc. 15 (2015) 828.
[6] V.C. Daniel, L. Marchionni, J.S. Hierman, J.T. Rhodes, W.L. Devereux,

C.M. Rudin, R. Yung, G. Parmigiani, M. Dorsch, C.D. Peacock, D.N. Watkins, A primary xenograft model of small-cell lung cancer reveals irreversible changes in gene expression imposed by culture in vitro, Canc. Res. 69 (8) (2009) 3364–3373.
[7] S.Y. Choi, D. Lin, P.W. Gout, C.C. Collins, Y. Xu, Y. Wang, Lessons from patient-derived xenografts for better in vitro modeling of human cancer, Adv. Drug Deliv. Rev. 79–80 (2014) 222–237.
[8] N. McGranahan, C. Swanton, Clonal heterogeneity and tumor evolution: past, present, and the future, Cell 168 (4) (2017) 613–628.
[9] Q. Gao, Z.C. Wang, M. Duan, Y.H. Lin, X.Y. Zhou, D.L. Worthley, X.Y. Wang, G. Niu, Y. Xia, M. Deng, L.Z. Liu, J.Y. Shi, L.X. Yang, S. Zhang, Z.B. Ding, J. Zhou, C.M. Liang, Y. Cao, L. Xiong, R. Xi, Y.Y. Shi, J. Fan, Cell culture system for analysis of genetic heterogeneity within hepatocellular carcinomas and response to pharmacologic agents, Gastroenterology 152 (1) (2017) 232–242 e4.
[10] J. Chaisaingmongkol, A. Budhu, H. Dang, S. Rabibhadana, B. Pupacdi, S.M. Kwon, M. Forgues, Y. Pomyen, V. Bhudhisawasdi, N. Lertprasertsuke, A. Chotirosniramit, C. Pairojkul, C.U. Auewarakul, T. Sricharunrat, K. Phornphutkul, S. Sangrajrang, M. Cam, P. He, S.M. Hewitt, K. Ylaya, X. Wu, J.B. Andersen, S.S. Thorgeirsson, J.J. Waterfall, Y.J. Zhu, J. Walling, H.S. Stevenson, D. Edelman, P.S. Meltzer, C.A. Loffredo, N. Hama, T. Shibata, R.H. Wiltrout, C.C. Harris, C. Mahidol, M. Ruchirawat, X.W. Wang, T.-L. Consortium, Common molecular subtypes among asian hepatocellular carcinoma and cholangiocarcinoma, Canc. Cell 32 (1) (2017) 57–70 e3.
[11] M. Hidalgo, F. Amant, A.V. Biankin, E. Budinska, A.T. Byrne, C. Caldas, R.B. Clarke, S. de Jong, J. Jonkers, G.M. Maelandsmo, S. Roman-Roman, J. Seoane, L. Trusolino, A. Villanueva, Patient-derived xenograft models: an emerging platform for translational cancer research, Canc. Discov. 4 (9) (2014) 998–1013.
[12] P.F. Cheung, C.W. Yip, L.W. Ng, K.W. Lo, C. Chow, K.F. Chan, T.T. Cheung, S.T. Cheung, Comprehensive characterization of the patient-derived xenograft and the paralleled primary hepatocellular carcinoma cell line, Canc. Cell Int. 16 (2016) 41.
[13] H. Xin, K. Wang, G. Hu, F. Xie, K. Ouyang, X. Tang, M. Wang, D. Wen, Y. Zhu, X. Qin, Establishment and characterization of 7 novel hepatocellular carcinoma cell lines from patient-derived tumor xenografts, PLos One 9 (1) (2014), e85308.
[14] H. Huynh, K.C. Soo, P.K. Chow, L. Panasci, E. Tran, Xenografts of human hepatocellular carcinoma: a useful model for testing drugs, Clin. Canc. Res. 12 (2006) 4306–4314 (14 Pt 1).
[15] B. Nugraha, X. Hong, X. Mo, L. Tan, W. Zhang, P.M. Chan, C.H. Kang, Y. Wang, L.T. Beng, W. Sun, D. Choudhury, J.M. Robens, M. McMillian, J. Silva, S. Dallas, C.H. Tan, Z. Yue, H. Yu, Galactosylated cellulosic sponge for multi-well drug safety testing, Biomaterials 32 (29) (2011) 6982–6994.
[16] Z. Yue, F. Wen, S. Gao, M.Y. Ang, P.K. Pallathadka, L. Liu, H. Yu, Preparation of three-dimensional interconnected macroporous cellulosic hydrogels for soft tissue engineering, Biomaterials 31 (32) (2010) 8141–8152.
[17] E.L.S. Fong, T.B. Toh, X. Lin, Z. Liu, L. Hooi, M.B. Mohd Abdul Rashid, T. Benoukraf, E.K.-H. Chow, T.H. Huynh, H. Yu, Data Describing the Growth and Molecular Features of Hepatocellular Carcinoma Patient-derived Xenograft Cells grown in a Three-dimensional Macroporous Hydrogel, Data In Brief, 2017.
[18] H. Huynh, K.H. Chow, K.C. Soo, H.C. Toh, S.P. Choo, K.F. Foo, D. Poon, V.C. Ngo, E. Tran, RAD001 (everolimus) inhibits tumour growth in xenograft models of human hepatocellular carcinoma, J. Cell Mol. Med. 13 (7) (2009) 1371–1380.
[19] H. Huynh, P.K. Chow, W.M. Tai, S.P. Choo, A.Y. Chung, H.S. Ong, K.C. Soo, R. Ong, R. Linnartz, M.M. Shi, Dovitinib demonstrates antitumor and anti-metastatic activities in xenograft models of hepatocellular carcinoma, J. Hepatol. 56 (3) (2012) 595–601.
[20] H. Huynh, V.C. Ngo, H.N. Koong, D. Poon, S.P. Choo, C.H. Thng, P. Chow, H.S. Ong, A. Chung, K.C. Soo, Sorafenib and rapamycin induce growth suppression in mouse models of hepatocellular carcinoma, J. Cell Mol. Med. 13 (8B) (2009) 2673–2683.
[21] H. Huynh, V.C. Ngo, H.N. Koong, D. Poon, S.P. Choo, H.C. Toh, C.H. Thng, P. Chow, H.S. Ong, A. Chung, B.C. Goh, P.D. Smith, K.C. Soo, AZD6244 enhances the anti-tumor activity of sorafenib in ectopic and orthotopic models of human hepatocellular carcinoma (HCC), J. Hepatol. 52 (1) (2010) 79–87.
[22] H. Li, R. Durbin, Fast and accurate short read alignment with Burrows-Wheeler transform, Bioinformatics 25 (14) (2009) 1754–1760.
[23] A. McKenna, M. Hanna, E. Banks, A. Sivachenko, K. Cibulskis, A. Kernytsky, K. Garimella, D. Altshuler, S. Gabriel, M. Daly, M.A. DePristo, The Genome Analysis Toolkit: a MapReduce framework for analyzing next-generation DNA sequencing data, Genome Res. 20 (9) (2010) 1297–1303.
[24] P. Danecek, A. Auton, G. Abecasis, C.A. Albers, E. Banks, M.A. DePristo, R.E. Handsaker, G. Lunter, G.T. Marth, S.T. Sherry, G. McVean, R. Durbin, G. Genomes Project Analysis, the variant call format and VCFtools, Bioinformatics 27 (15) (2011) 2156–2158.
[25] K. Wang, M. Li, H. Hakonarson, ANNOVAR: functional annotation of genetic variants from high-throughput sequencing data, Nucleic Acids Res. 38 (16) (2010) e164.
[26] A. Dobin, C.A. Davis, F. Schlesinger, J. Drenkow, C. Zaleski, S. Jha, P. Batut, M. Chaisson, T.R. Gingeras, STAR: ultrafast universal RNA-seq aligner, Bioinformatics 29 (1) (2013) 15–21.
[27] S. Heinz, C. Benner, N. Spann, E. Bertolino, Y.C. Lin, P. Laslo, J.X. Cheng, C. Murre, H. Singh, C.K. Glass, Simple combinations of lineage-determining transcription factors prime cis-regulatory elements required for macrophage and B cell identities, Mol. Cell 38 (4) (2010) 576–589.
[28] D.W. Ho, A.K. Kai, I.O. Ng, TCGA whole-transcriptome sequencing data reveals significantly dysregulated genes and signaling pathways in hepatocellular carcinoma, Front. Med. 9 (3) (2015) 322–330.
[29] M. Kanehisa, S. Goto, KEGG: kyoto encyclopedia of genes and genomes, Nucleic Acids Res. 28 (1) (2000) 27–30.
[30] E. Curcio, S. Salerno, G. Barbieri, L. De Bartolo, E. Drioli, A. Bader, Mass transfer and metabolic reactions in hepatocyte spheroids cultured in rotating wall gas-permeable membrane system, Biomaterials 28 (36) (2007) 5487–5497.
[31] H.K. Chang, Y.J. Park, H. Koh, S.M. Kim, K.S. Chung, J.T. Oh, S.J. Han, Hepatic fibrosis scan for liver stiffness score measurement: a useful preendoscopic screening test for the detection of varices in postoperative patients with biliary atresia, J. Pediatr. Gastroenterol. Nutr. 49 (3) (2009) 323–328.
[32] C.S. Cho, S.J. Seo, I.K. Park, S.H. Kim, T.H. Kim, T. Hoshiba, I. Harada, T. Akaike, Galactose-carrying polymers as extracellular matrices for liver tissue engineering, Biomaterials 27 (4) (2006) 576–585.
[33] L.B. Alexandrov, S. Nik-Zainal, D.C. Wedge, S.A. Aparicio, S. Behjati, A.V. Biankin, G.R. Bignell, N. Bolli, A. Borg, A.L. Borresen-Dale, S. Boyault, B. Burkhardt, A.P. Butler, C. Caldas, H.R. Davies, C. Desmedt, R. Eils, J.E. Eyfjord, J.A. Foekens, M. Greaves, F. Hosoda, B. Hutter, T. Ilicic, S. Imbeaud, M. Imielinski, N. Jager, D.T. Jones, D. Jones, S. Knappskog, M. Kool, S.R. Lakhani, C. Lopez-Otin, S. Martin, N.C. Munshi, H. Nakamura, P.A. Northcott, M. Pajic, E. Papaemmanuil, A. Paradiso, J.V. Pearson, X.S. Puente, K. Raine, M. Ramakrishna, A.L. Richardson, J. Richter, P. Rosenstiel, M. Schlesner, T.N. Schumacher, P.N. Span, J.W. Teague, Y. Totoki, A.N. Tutt, R. Valdes-Mas, M.M. van Buuren, L. van 't Veer, A. Vincent-Salomon, N. Waddell, L.R. Yates, I. Australian Pancreatic Cancer Genome, I.B.C. Consortium, I.M.-S. Consortium, I. PedBrain, J. Zucman-Rossi, P.A. Futreal, U. McDermott, P. Lichter, M. Meyerson, S.M. Grimmond, R. Siebert, E. Campo, T. Shibata, S.M. Pfister, P.J. Campbell, M.R. Stratton, Signatures of mutational processes in human cancer, Nature 500 (7463) (2013) 415–421.
[34] J.M. Llovet, S. Ricci, V. Mazzaferro, P. Hilgard, E. Gane, J.F. Blanc, A.C. de Oliveira, A. Santoro, J.L. Raoul, A. Forner, M. Schwartz, C. Porta, S. Zeuzem, L. Bolondi, T.F. Greten, P.R. Galle, J.F. Seitz, I. Borbath, D. Haussinger, T. Giannaris, M. Shan, M. Moscovici, D. Voliotis, J. Bruix, S.I.S. Group, Sorafenib in advanced hepatocellular carcinoma, N. Engl. J. Med. 359 (4) (2008) 378–390.
[35] B. Schmidt, L. Wei, D.K. DePeralta, Y. Hoshida, P.S. Tan, X. Sun, J.P. Sventek, M. Lanuti, K.K. Tanabe, B.C. Fuchs, Molecular subclasses of hepatocellular carcinoma predict sensitivity to fibroblast growth factor receptor inhibition, Int. J. Canc. 138 (6) (2016) 1494–1505.
[36] T. Scheller, C. Hellerbrand, C. Moser, K. Schmidt, A. Kroemer, S.M. Brunner, H.J. Schlitt, E.K. Geissler, S.A. Lang, mTOR inhibition improves fibroblast growth factor receptor targeting in hepatocellular carcinoma, Br. J. Canc. 112 (5) (2015) 841–850.
[37] H. Gao, J.M. Korn, S. Ferretti, J.E. Monahan, Y. Wang, M. Singh, C. Zhang, C. Schnell, G. Yang, Y. Zhang, O.A. Balbin, S. Barbe, H. Cai, F. Casey, S. Chatterjee, D.Y. Chiang, S. Chuai, S.M. Cogan, S.D. Collins, E. Dammassa, N. Ebel, M. Embry, J. Green, A. Kauffmann, C. Kowal, R.J. Leary, J. Lehar, Y. Liang, A. Loo, E. Lorenzana, E. Robert McDonald 3rd, M.E. McLaughlin, J. Merkin, R. Meyer, T.L. Naylor, M. Patawaran, A. Reddy, C. Roelli, D.A. Ruddy, F. Salangsang, F. Santacroce, A.P. Singh, Y. Tang, W. Tinetto, S. Tobler, R. Velazquez, K. Venkatesan, F. Von Arx, H.Q. Wang, Z. Wang, M. Wiesmann, D. Wyss, F. Xu, H. Bitter, P. Atadja, E. Lees, F. Hofmann, E. Li, N. Keen, R. Cozens, M.R. Jensen, N.K. Pryer, J.A. Williams, W.R. Sellers, High-throughput screening using patient-derived tumor xenografts to predict clinical trial drug response, Nat. Med. 21 (11) (2015) 1318–1325.
[38] A. Bruna, O.M. Rueda, W. Greenwood, A.S. Batra, M. Callari, R.N. Batra, K. Pogrebniak, J. Sandoval, J.W. Cassidy, A. Tufegdzic-Vidakovic, S.J. Sammut, L. Jones, E. Provenzano, R. Baird, P. Eirew, J. Hadfield, M. Eldridge, A. McLaren-Douglas, A. Barthorpe, H. Lightfoot, M.J. O'Connor, J. Gray, J. Cortes, J. Baselga, E. Marangoni, A.L. Welm, S. Aparicio, V. Serra, M.J. Garnett, C. Caldas, A biobank of breast cancer explants with preserved intra-tumor heterogeneity to screen anticancer compounds, Cell 167 (1) (2016) 260–274 e22.
[39] E.L. Fong, M. Martinez, J. Yang, A.G. Mikos, N.M. Navone, D.A. Harrington, M.C. Farach-Carson, Hydrogel-based 3D model of patient-derived prostate xenograft tumors suitable for drug screening, Mol. Pharm. 11 (7) (2014) 2040–2050.
[40] Z. Qiu, K. Zou, L. Zhuang, J. Qin, H. Li, C. Li, Z. Zhang, X. Chen, J. Cen, Z. Meng, H. Zhang, Y. Li, L. Hui, Hepatocellular carcinoma cell lines retain the genomic and transcriptomic landscapes of primary human cancers, Sci. Rep. 6 (2016) 27411.
[41] E.L. Fong, S.E. Lamhamedi-Cherradi, E. Burdett, V. Ramamoorthy, A.J. Lazar, F.K. Kasper, M.C. Farach-Carson, D. Vishwamitra, E.G. Demicco, B.A. Menegaz, H.M. Amin, A.G. Mikos, J.A. Ludwig, Modeling Ewing sarcoma tumors in vitro with 3D scaffolds, Proc. Natl. Acad. Sci. U. S. A. 110 (16) (2013) 6500–6505.
[42] C. Fischbach, R. Chen, T. Matsumoto, T. Schmelzle, J.S. Brugge, P.J. Polverini, D.J. Mooney, Engineering tumors with 3D scaffolds, Nat. Med. 4 (10) (2007) 855–860.
[43] T. Jacks, R.A. Weinberg, Taking the study of cancer cell survival to a new dimension, Cell 111 (7) (2002) 923–925.
[44] H.R. Jung, H.M. Kang, J.W. Ryu, D.S. Kim, K.H. Noh, E.S. Kim, H.J. Lee, K.S. Chung, H.S. Cho, N.S. Kim, D.S. Im, J.H. Lim, C.R. Jung, Cell spheroids with enhanced aggressiveness to mimic human liver cancer in vitro and in vivo, Sci.

Rep. 7 (1) (2017) 10499.
[45] A. Takai, V. Fako, H. Dang, M. Forgues, Z. Yu, A. Budhu, X.W. Wang, Three-dimensional organotypic culture models of human hepatocellular carcinoma, Sci. Rep. 6 (2016) 21174.
[46] M.J. Gomez-Lechon, L. Tolosa, I. Conde, M.T. Donato, Competency of different cell models to predict human hepatotoxic drugs, Expet Opin. Drug Metabol. Toxicol. 10 (11) (2014) 1553–1568.
[47] M. van de Wetering, H.E. Francies, J.M. Francis, G. Bounova, F. Iorio, A. Pronk, W. van Houdt, J. van Gorp, A. Taylor-Weiner, L. Kester, A. McLaren-Douglas, J. Blokker, S. Jaksani, S. Bartfeld, R. Volckman, P. van Sluis, V.S. Li, S. Seepo, C. Sekhar Pedamallu, K. Cibulskis, S.L. Carter, A. McKenna, M.S. Lawrence, L. Lichtenstein, C. Stewart, J. Koster, R. Versteeg, A. van Oudenaarden, J. Saez-Rodriguez, R.G. Vries, G. Getz, L. Wessels, M.R. Stratton, U. McDermott, M. Meyerson, M.J. Garnett, H. Clevers, Prospective derivation of a living organoid biobank of colorectal cancer patients, Cell 161 (4) (2015) 933–945.
[48] M. Schutte, T. Risch, N. Abdavi-Azar, K. Boehnke, D. Schumacher, M. Keil, R. Yildiriman, C. Jandrasits, T. Borodina, V. Amstislavskiy, C.L. Worth, C. Schweiger, S. Liebs, M. Lange, H.J. Warnatz, L.M. Butcher, J.E. Barrett, M. Sultan, C. Wierling, N. Golob-Schwarzl, S. Lax, S. Uranitsch, M. Becker, Y. Welte, J.L. Regan, M. Silvestrov, I. Kehler, A. Fusi, T. Kessler, R. Herwig, U. Landegren, D. Wienke, M. Nilsson, J.A. Velasco, P. Garin-Chesa, C. Reinhard, S. Beck, R. Schafer, C.R. Regenbrecht, D. Henderson, B. Lange, J. Haybaeck, U. Keilholz, J. Hoffmann, H. Lehrach, M.L. Yaspo, Molecular dissection of colorectal cancer in pre-clinical models identifies biomarkers predicting sensitivity to EGFR inhibitors, Nat. Commun. 8 (2017) 14262.
[49] M. Fujii, M. Shimokawa, S. Date, A. Takano, M. Matano, K. Nanki, Y. Ohta, K. Toshimitsu, Y. Nakazato, K. Kawasaki, T. Uraoka, T. Watanabe, T. Kanai, T. Sato, A colorectal tumor organoid library demonstrates progressive loss of niche factor requirements during tumorigenesis, Cell Stem Cell 18 (6) (2016) 827–838.
[50] S.D. Wu, Y.S. Ma, Y. Fang, L.L. Liu, D. Fu, X.Z. Shen, Role of the microenvironment in hepatocellular carcinoma development and progression, Canc. Treat Rev. 38 (3) (2012) 218–225.